Inorg. Chem. **2003**, *42*, 3466–3474

Coordination Properties of a Diarylaza Crown Ether Appended with a Luminescent $[Ru(bipy)_3]^{2+}$ Unit

Loïc J. Charbonnière,*,† Raymond F. Ziessel,*,† Craig A. Sams,‡ and Anthony Harriman‡

Laboratoire de Chimie Moléculaire, UMR 7008 au CNRS, Ecole de Chimie, Polymère et Matériaux, 25, rue Becquerel, 67087 Strasbourg, Cedex 02, France, and Molecular Photonics Laboratory, School of Natural Sciences, Bedson Building, University of Newcastle, Newcastle upon Tyne, NE1 7RU, U.K.

Received November 13, 2002

The $[Ru(bipy)_2(\mathbf{1})](PF_6)_2$ (bipy refers to 2,2′-bipyridine) complex, comprising a ruthenium(II) tris(2,2′-bipyridine) luminophore covalently linked to a di[(*o*-triethyleneglycoxy)phenyl]amine crown ether **1**, has been synthesized and fully characterized. The photophysical properties of this metal complex have been examined in solution at ambient temperature. Luminescence from the metal complex is enhanced significantly in the presence of various adventitious cations, including protons. In particular, Li^+ cations bind to the crown ether, as evidenced by ^1H NMR and luminescence spectroscopy. Cation binding serves to decrease the rate of reductive quenching of the triplet state of the metal complex, thereby increasing the extent of luminescence. The solution-phase conformation of $[Ru(bipy)_2(\mathbf{1})](PF_6)_2$, with and without encapsulated Li^+, has been examined by 2-D NMR and by molecular dynamics simulations.

Introduction

There is currently a considerable effort devoted to the design and synthesis of selective luminophores aimed at recognizing and signaling the presence of substrates, such as neutral molecules or ions.[1−3] Such molecular sensors are usually constructed by combining a complexation pocket, designed for the specific binding of an incoming substrate, with a luminescent fragment whose photophysical properties are perturbed during the recognition process, so as to produce a measurable output signal. Many diverse approaches are available by which to monitor the complexation step, including changes in absorption spectral profile,[4] modulation of the refractive index,[5] or perturbation of the emission intensity. The latter approach has the added attraction of extremely high sensitivity and, by using time-resolved luminescence techniques, of providing additional information about the binding event. It is also apparent that the time scale of the luminescence process can be tuned over an inordinately wide range by proper selection of the luminophore. Thus, organic substrates can be used for fluorescence studies in the nanosecond to picosecond time range,[6] and d-block transition metal complexes often exhibit room-temperature phosphorescence over the microsecond time range,[7] while certain lanthanide complexes emit on the millisecond time scale.[8] Each of these events has particular applications in the field of chemical sensors.

Translation of the binding event into a spectral change can be effected in one of two ways: First, attachment of the substrate could induce a major conformational change in the sensor−substrate adduct that forces the two subunits to adopt markedly different relative positions. This structural reorganization can modulate the effectiveness of through-space

* Authors to whom correspondence should be addressed. E-mail: ziessel@chimie.u-strasbg.fr (R.F.Z.).
† Ecole de Chimie, Polymère et Matériaux.
‡ University of Newcastle.

(1) De Silva, A. P.; Gunaratne, H. Q. N.; Gunnlaugsson, T.; Huxley, A. J. M.; McCoy, C. P.; Rademacher, J. T.; Rice, T. E. *Chem. Rev.* **1997**, *97*, 1515.
(2) *Fluorescent Chemosensors for Ion and Molecule Recognition*; Czarnik, A. W., Ed.; American Chemical Society: Washington, DC, 1992.
(3) Beer, P. D.; Gale, P. A. *Angew. Chem., Int. Ed.* **2001**, *40*, 486.
(4) Aït-Haddou, H.; Wiskur, S. L.; Lynch, V. M.; Anslyn, E. V. *J. Am. Chem. Soc.* **2001**, *123*, 11296.
(5) Mines, G. A.; Tzeng, B.-C.; Stevenson, K. J.; Li, J.; Hupp, J. T. *Angew. Chem., Int. Ed.* **2002**, *41*, 154.
(6) Mayer, A.; Neuenhofer, S. *Angew. Chem., Int. Ed. Engl.* **1994**, *33*, 1044.
(7) Anzenbacher, P., Jr.; Tyson, D. S.; Jursikova, K.; Castellano, F. N. *J. Am. Chem. Soc.* **2002**, *124*, 6232.
(8) (a) Montaldi, M.; Prodi, L.; Zaccheroni, N.; Charbonnière, L. J.; Douce, L.; Ziessel, R. *J. Am. Chem. Soc.* **2001**, *123*, 12694. (b) Charbonnière, L. J.; Ziessel, R.; Montaldi, M.; Prodi, L.; Zaccheroni, N.; Boehme, C.; Wipff, G. *J. Am. Chem. Soc.* **2002**, *124*, 7779. (c) Bruce, J. I.; Dickins, R. S.; Govenlock, L. J.; Gunnlaugsson, T.; Lopinski, S.; Lowe, M. P.; Parker, D.; Peacock, R. D.; Perry, J. J. B.; Aime, S.; Botta, M. *J. Am. Chem. Soc.* **2000**, *122*, 9674.

10.1021/ic020671t CCC: $25.00
Published on Web 04/30/2003

Scheme 1. Hydrogen Labeling in the $[Ru(bipy)_2 \cdot 1]^{2+}$ Complex[a]

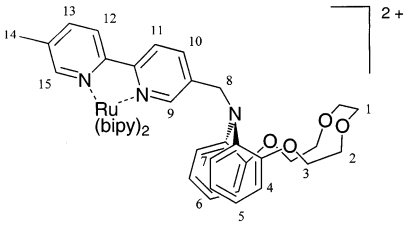

[a] bipy represents 2,2′-bipyridine.

interactions, such as short-range electron transfer, magnetic coupling, or long-range energy transfer. The programmed inducement of changes in molecular geometry provides the basic operating principle for luminescent probes such as molecular beacons[9] and resonance energy transfer protocols.[10−12] Second, the binding process can alter the electronic properties of the adduct such that intramolecular electron-transfer processes become favored or disfavored. Typical examples of this latter approach include the complexation of highly charged species,[13] and the modulation of excimer[14] or exciplex[15] interactions by the presence of a substrate. In cases where the sensor and trap are linked by a rigid connector, the binding process can be detected by through-bond interactions,[16] since conformational changes are minimized, but in most examples the overall binding-recognition event involves a combination of conformational and electronic reorganization within the adduct.[17]

In attempting to expand the known field of chemical sensors, we have designed a new system around ligand **1**.[18] This sensor comprises a di[(*o*-triethyleneglycoxy)phenyl]-amine crown ether functionalized with a methylene-bridged 2,2′-bipyridine unit that allows facile attachment of a ruthenium(II) bis(2,2′-bipyridine) fragment (Scheme 1). Clearly, the crown ether is intended to serve as the trap for cations in solution and the metal complex is supposed to provide the output signal. The short connector has been selected so as to reduce conformational mobility and to maintain the two subunits in close electronic partnership throughout the binding process.

Experimental Section

Starting Materials and General Procedures. Solvents and raw materials were of analytical grade and were used as received. An exception was acetonitrile, which was filtered over activated alumina (Merck) and distilled from P_2O_5 under an argon atmosphere immediately prior to use.[19] Samples of $[Ru(bipy)_2Cl_2] \cdot 2H_2O$,[20] together with compounds **1** and **4**,[18] were synthesized according to literature procedures.

1- and 2-D ^1H NMR (200 and 400 MHz) and ^{13}C NMR (50 or 100 MHz) spectra were recorded with Brüker AC200 and AMX400 spectrometers, using perdeuterated solvents as internal standards. FT-IR spectra were obtained from KBr pellets on a Nicolet 210 spectrometer. Fast-atom bombardment (FAB, positive mode) mass spectra were recorded using *m*-nitrobenzyl alcohol as matrix. Absorption spectra were recorded on a Uvikon 933 spectrophotometer, using 1 cm path length quartz cells. Fluorescence and corrected excitation spectra were recorded on a Perkin-Elmer LS 50 spectrometer using deoxygenated anhydrous acetonitrile as solvent. Spectroscopic titrations were carried out at constant ionic strength using 0.01 M tetra-*n*-butylammonium perchlorate, the latter being freshly recrystallized. Luminescence quantum yields were measured relative to $[Ru(bipy)_3](PF_6)_2$ in deoxygenated acetonitrile as standard.[21] Luminescence lifetimes were measured by time-resolved emission spectroscopy following excitation at 532 nm with a 5 ns laser pulse. The sample was dissolved in deoxygenated acetonitrile, and emission was isolated from scattered laser light using a high-radiance monochromator. Approximately 512 individual laser shots were averaged prior to data analysis.

Transient absorption spectra were recorded point-by-point after excitation of the compound in deoxygenated acetonitrile with a 10 ns laser pulse at 532 nm. The probing beam was supplied with a pulsed, high-intensity xenon arc lamp passed through the solution at 90° to the excitation beam. The monitoring beam was directed onto the entrance slits of a Spex high-radiance monochromator and then to a fast response photomultiplier. The signal was stored in a transient recorder, sent to a PC, and averaged. Approximately 100 individual laser shots were averaged at each monitoring wavelength and used to construct the differential absorption spectrum. The reported spectrum was recorded 50 ns after the excitation pulse.

Electrochemical studies were made by cyclic voltammetry using a conventional three-electrode setup on a BAS CV-50W voltammetric analyzer equipped with a Pt microdisk working electrode and a silver wire counter electrode. Ferrocene was used as an internal standard and was calibrated against a saturated calomel reference electrode (SSCE) separated from the electrolysis cell by a glass frit presoaked with electrolyte. Solutions contained the electroactive substrate (ca. 2×10^{-4} M) in deoxygenated anhydrous acetonitrile containing tetra-*n*-butylammonium tetrafluoroborate (0.2 M) as supporting electrolyte. The quoted half-wave potentials were reproducible to within 20 mV.

(9) Zhang, P.; Beck, T.; Tan, W. *Angew. Chem., Int Ed.* **2001**, *40*, 402.
(10) (a) Arai, R.; Nakagawa, H.; Tsumoto, K.; Mahoney, W.; Kumagai, I.; Ueda, H.; Nagamune, T. *Anal. Biochem.* **2001**, *289*, 77. (b) Xu, Y.; Piston, D. W.; Hirschie Johnson, C. *Proc. Natl. Acad. Sci. U.S.A.* **1999**, *96*, 151.
(11) (a) Arai, R.; Ueda, H.; Tsumoto, K.; Mahoney, W. C.; Kumagai, I.; Nagamune, T. *Protein Eng.* **2000**, *13*, 369. (b) Sagot, I.; Bonneu, M.; Balguerie, A.; Aigle, A. *FEBS Lett.* **1999**, *447*, 53.
(12) Selvin, P. R.; Hearst, J. E. *Proc. Natl. Acad. Sci. U.S.A.* **1994**, *116*, 6029.
(13) For recent examples see: (a) Hirano, T.; Kikuchi, K.; Urano, Y.; Higuchi, T.; Nagano, T. *Angew. Chem., Int. Ed.* **2000**, *39*, 1052. (b) Cox, B. G.; Hurwood, T. V.; Prodi, L.; Montalti, M.; Bolletta, F.; Watt, C. I. F. *J. Chem. Soc., Perkin Trans. 2* **1999**, 289. (c) Tahri, A.; Cielen, E.; van Aken, K. J.; Hoornaert, G. J.; de Schryver, F. C.; Boens, N.; *J. Chem. Soc., Perkin Trans. 2* **1999**, 1739.
(14) (a) Marquis, D.; Desvergne, J.-P. *Chem. Phys. Lett.* **1994**, *230*, 131. (b) Marquis, D.; Desvergne, J.-P.; Bouas-Laurent, H. *J. Org. Chem.* **1995**, *60*, 7984.
(15) (a) Simeonov, A.; Matsushita, M.; Juban, E. A.; Thompson, E. H. Z.; Hoffman, T. Z.; Beuscher, A. E., IV; Taylor, M. J.; Wirsching, P.; Rettig, W.; McCusker, J. K.; Stevens, R. C.; Millar, D. P.; Schultz, P. G.; Lerner, R. A.; Janda, K. D. *Science* **2000**, *290*, 307. (b) Nishizawa, S.; Watanabe, M.; Uchida, T.; Teramae, N. *J. Chem. Soc., Perkin Trans. 2* **1999**, 141.
(16) (a) Barigelletti, F.; Flamigni, L.; Guardigli, M.; Sauvage, J.-P.; Collin, J.-P.; Sour, A. *Chem. Commun.* **1996**, 1329. (b) Ziessel, R.; Hissler, M.; El-ghayoury, A.; Harriman, A. *Coord. Chem. Rev.* **1998**, *178−180*, 1251.
(17) (a) Harriman, A.; Hissler, M.; Jost, P.; Wipff, G.; Ziessel, R. *J. Am. Chem. Soc.* **1999**, *121*, 14. (b) Weinig, H.-G.; Krauss, R.; Seydack, M.; Bendig, J.; Koert, U. *Chem. Eur. J.* **2001**, *7*, 2075.
(18) Charbonnière, L. J.; Ziessel, R. F. *Tetrahedron Lett.* **2000**, *41*, 2373.
(19) Perrin, D. D.; Armarego, W. L. F. In *Purification of Laboratory Chemicals*, 3rd ed.; Pergamon Press: New York, 1988.
(20) Sprintschnik, G.; Sprintschnik, H. W.; Kirsch P. P.; Whitten, D. *J. Am. Chem. Soc.* **1977**, *99*, 4947.
(21) Caspar, J. V.; Meyer, T. J. *J. Am. Chem. Soc.* **1983**, *105*, 5583.

Scheme 2[a]

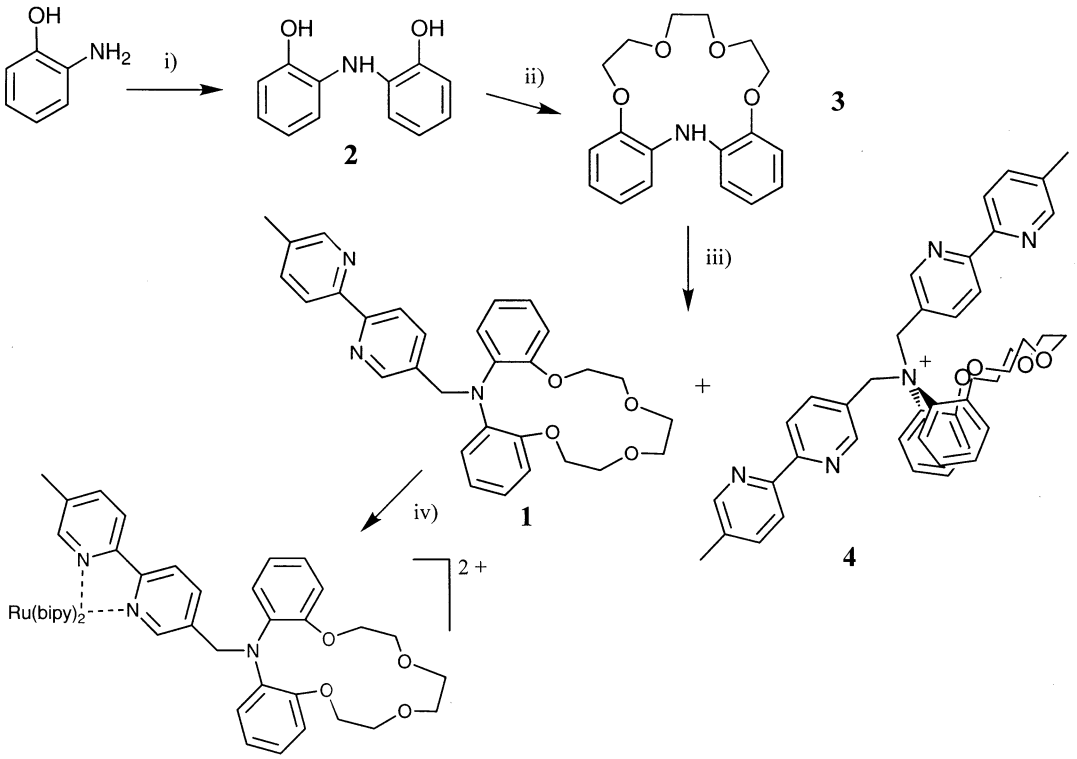

[a] (i) HCl 0.5 equiv, melted salt 240 °C, 39%; (ii) $TsOCH_2(CH_2OCH_2)_2CH_2OTs$, Cs_2CO_3, CH_3CN, 80 °C, 68%; (iii) 5-methyl-5′-bromomethyl-2,2′-bipyridine, 1.1 equiv, K_2CO_3, CH_3CN, 80 °C, 38%; (iv) $[Ru(bipy)_2Cl_2]$, EtOH, 80 °C, 55%.

Molecular dynamics calculations were carried out using the Discover 3 module available in Insight II running on a Silicon Graphics O2 workstation. For all calculations, partial charges were assigned using the ESFF force field. Optimized geometries were obtained using the Newton method, and subsequent molecular dynamics calculations were performed over a period of 200 ps with a step function of 1 fs. A 30 × 30 × 30 Å^3 solvent box containing 256 acetonitrile molecules was applied to the calculations with Li^+ cations.

Synthesis of $[Ru(bipy)_2(1)](PF_6)_2$. A solution of **1** (33 mg, 0.066 mmol) and $[Ru(bipy)_2Cl_2]\cdot 2H_2O$ (34 mg, 0.066 mmol) in 10 mL of Ar-deoxygenated ethanol was heated at 80 °C for 17 h in a Schlenck tube under an Ar atmosphere. After cooling to room temperature, 5 mL of water containing KPF_6 (40 mg, 0.2 mmol) was added to the solution, which was concentrated under reduced pressure until a precipitate formed. The orange residue was recovered by centrifugation, dried under vacuum, and purified by column chromatography on alumina using a mixture of CH_2Cl_2/MeOH (97/3 v/v) as eluent to give the complex (40 mg, 55%) as an orange solid. ^{1}H NMR (CD_3CN, 200 MHz): δ 2.16 (s, 3H), 3.51−3.55 (m, 4H), 3.60 (s, 4H), 3.94−3.98 (m, 4H), 4.71 (s, 2H), 6.57−6.73 (m, 4H), 6.82−6.99 (m, 4H), 7.31−7.36 (m, 5H), 7.42 (s, br, 2H), 7.56 (d, 1H, ^3J = 5.5 Hz), 7.66 (t, br, 2H, ^3J = 6.5 Hz), 7.82 (d, br, 1H, ^3J = 8.5 Hz), 7.96−8.11 (m, 4H), 8.24−8.34 (m, 2H), 8.41−8.49 (m, 4H), 8.62 (d, br, 1H, ^3J = 8.5 Hz). ^{13}C NMR (CD_3CN, 100 MHz): δ 17.9, 53.0, 67.8, 68.9, 69.4, 114.1, 120.9, 123.7, 123.9, 124.2, 124.6, 124.7 (2C), 127.7, 127.9 (2C), 128.0, 137.9, 138.0, 138.1, 138.7, 138.8, 139.4, 140.7, 150.1, 151.6, 151.8, 151.9, 152.0, 152.9, 154.7, 155.7, 157.2 (2C), 157.4, 157.5. FAB$^+$-MS: $[Ru\cdot\mathbf{1}]^{+\bullet}$ 911 (100%, calcd 911.7), $[Ru\cdot\mathbf{1}](PF_6)^+$ 1056 (45% calcd 1056.6). IR (KBr, cm^{-1}) 2923 (C−H), 1499, 1465, 1447 (C═C, C═N), 1255, 840 (PF_6), 557 (PF_6). Elemental anal. Found: C, 49.89; H, 3.79; N, 8.05. Calcd for $C_{50}F_{12}H_{47}N_7O_4P_2Ru$: C, 50.01; H, 3.94; N, 8.16. R_f = 0.38 (SiO_2, CH_2Cl_2/MeOH, 95/5, v/v).

Results

Synthesis and Characterization. The free ligand **1** was obtained in three steps according to Scheme 2. Self-condensation of *o*-aminophenol in a molten salt, using conditions adapted from literature procedures,[22] afforded the intermediate di(*o*-hydroxyphenyl)amine, **2**. This compound was reacted with the ditosyl derivative of triethyleneglycol[23] to give the corresponding diarylamine-based crown ether **3** in 55% yield. Nucleophilic substitution of this secondary amine with 5-bromomethyl-5′-methyl-2,2′-bipyridine[24] provided entry to the required ligand **1,** as well as to minor amounts of the quarternary ammonium salt, **4**. The yield of this latter compound was found to depend markedly on the relative concentration of the alkylating agent used.

The quaternary ammonium salt **4** is of special interest because its ^{1}H NMR spectrum provides key information about the chemical shift of the magnetically inequivalent bipy units (Figure 1). Thus, **4** exhibits a plane of symmetry passing through the N atom of the arylamine and bisecting the planes formed by the aromatic rings of the crown ether. Two sets of signals were observed for the protons of the bipy groups, clearly indicative of their residing in different chemical environments. This situation is particularly apparent for the

(22) De Antoni, J. *Bull. Soc. Chim. Fr.* **1963**, 2871.
(23) Ouchi, M.; Inoue, Y.; Kanzaki, T.; Hakushi, T. *J. Org. Chem.* **1984**, *49*, 1408.
(24) Ziessel, R.; Hissler, M.; Ulrich, G. *Synthesis* **1998**, 1339.

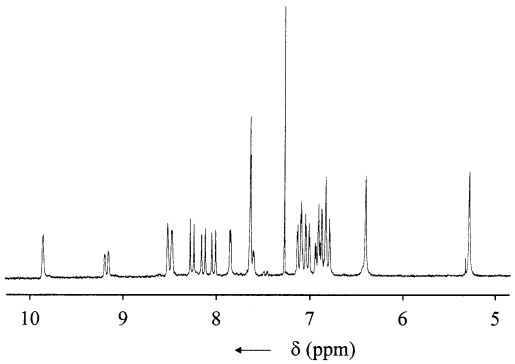

Figure 1. Methylenic and aromatic region of the ^{1}H NMR spectrum recorded for the ammonium salt **4** in $CDCl_3$ solution.

signals assigned to the methylene protons at 5.25 and 6.38 ppm in **4**, compared to the corresponding signal seen at 4.82 ppm for the free ligand **1**. Although the positive charge on the N atom is expected to induce a deshielding effect on these signals,[25] it seems unreasonable to suppose that this effect could cause a shift to 6.38 ppm. The schematic representation of **4** shown in Scheme 1 suggests that one bipy group is located immediately above the crown ether while the second bipy unit is directed away from the crown ether. On the basis of 2-D ^{1}H NMR COSY and NOESY experiments, it appears that the peak at 5.25 ppm is due to the methylene group that points away from the crown ether. For this signal, an NOE effect shows through-space correlation with H7 (δ = 7.10 ppm), thereby confirming its assignment.

The signals of the three protons of the pyridyl ring linked to this methylene bridge are strongly affected by the adjacent phenylene rings and are shifted to 7.81 ppm for H9 (7.43 ppm in **1**), 6.85 ppm for H10 (8.62 ppm in **1**), and 7.99 ppm for H11 (8.26 ppm in **1**). Its chemical environment also affects the signals seen for the second bipyridyl group. The methylene bridge is shifted downfield and occurs at 6.38 ppm. The aromatic protons on the adjacent pyridyl ring undergo a remarkable downfield shift of 2.46 ppm for H9′ (where prime refers to the second bipyridyl arm in the ammonium compound **4**) at 9.89 ppm, 0.59 ppm for H10′ (δ = 9.21 ppm), while H11′ remained unperturbed at 8.26 ppm. Such strong effects, and particularly that for H9′, may be explained by its presence in the deshielding regions of the aromatic benzene rings and/or by interactions with the lone pairs of the nitrogen and oxygen atoms of the crown ether.

The ruthenium complex of **1** was isolated as its PF_6^- salt in 55% yield, after treatment of **1** with 1 equiv of [Ru(bipy)$_2$Cl$_2$]·2H$_2$O in refluxing ethanol. The required compound was isolated by anion metathesis with KPF_6 and purification by column chromatography. Elemental analysis of the complex was in excellent agreement with the proposed structure of [Ru(bipy)$_2$(**1**)](PF$_6$)$_2$. The infrared spectrum of the complex in a KBr matrix displays bands at 840 and 558 cm^{-1} characteristic of the ν_3 and ν_4 IR active transitions of the unbound PF_6^- anion.[26] The presence of **1** is evidenced by a medium absorption band at 2923 cm^{-1}, together with a broad band centered at 2860 cm^{-1} that can be attributed to asymmetric and symmetric vibrational modes of the methyl and methylene groups.[27] At 1255 cm^{-1}, a strong absorption is observed which is tentatively assigned to either the $C_{aro}-N_{amine}$ or $C_{aro}-O_{ether}$ vibrations. The proposed stoichiometry is in agreement with the FAB$^+$ mass spectra, where peaks are observed at 1056 (45%), 911 (100%), and 597 (69%), corresponding respectively to the [M − PF$_6$]$^+$ monocation, the [M − 2PF$_6$] radical cation, and the [Ru(bipy)$_2$(Me-bipy-CH$_2$)]$^{+\bullet}$ radical cation arising from the fragmentation of the complex after loss of the crown ether.

Table 1. ^{1}H NMR Chemical Shifts for [Ru(bipy)$_2$(**1**)]$^{2+}$ and the Corresponding Lithium Complex

proton	[Ru(bipy)$_2$(**1**)]$^{2+}$	[Ru(bipy)$_2$(**1**)]$^{2+}$ + Li$^+$	$\Delta\delta^a$
1	3.60	3.65−3.72	−0.08
2	3.50−3.56	3.50−3.59	−0.02
3	3.93−4.00	3.62−3.68, 3.86−3.93	0.31, 0.07
4	6.84	6.75	0.09
5	6.95	7.06	−0.11
6	6.69	6.82	−0.13
7	6.59	6.87	−0.28
8	4.72	4.54	0.18
9	7.43	7.19	0.24
10	8.62	8.23	−0.39
11	8.26	8.40	−0.14
12	8.32	8.38	−0.06
13	7.82	7.84	−0.02
14	2.20	2.19	0.01
15	7.43	7.45	−0.02

^{a} $\Delta\delta = \delta_{free} - \delta_{Li}$.

The ^{1}H NMR spectrum recorded in CD_3CN provides strong indications for the solution-phase structure of the metal complex. The aliphatic region indicates a local plane of symmetry for protons associated with the crown ether. This finding implies that the chiral ruthenium center has little influence on these protons. Apart from the phenylene protons, the aromatic region displays a complicated pattern due to protons on the bipyridyl groups. However, on the basis of 2-D COSY and NOESY spectra, it has been possible to fully assign all the protons of ligand **1** in the metal complex (Table 1). An interesting feature of the NOESY spectrum is an unexpected correlation between the doublet of H7 seen at 6.59 ppm and the broad singlet at 7.43 ppm, which is assigned to the equivalent H9 and H15 protons (see Scheme 1 for numbering). A simple consideration of the relative distances involved suggests that there should be minimal dipolar correlation between H7 and H15, thereby indicating through-space proximity between H7 and H9. Furthermore, this spatial proximity is in keeping with molecular dynamics calculations which reveal the close spacing of these protons in the two most favored conformations of the metal complex (vide infra).

Other dipolar correlations are apparent in the spectrum. In particular, the correlation between H4 and H3 allows exact

(25) Gutsche, D. C.; Iqbal, M.; Alam, I. *J. Am. Chem. Soc.* **1987**, *109*, 4314.

(26) Nakamoto, K. *Infrared and Raman Spectra of Inorganic and Coordination Compounds*, 4th ed.; Wiley: New York, 1986; p 147.

(27) Silverstein, R. M.; Bassler, G. C. *Identification spectrométrique des composés organiques*; Gauthier-Villars: Paris, 1968.

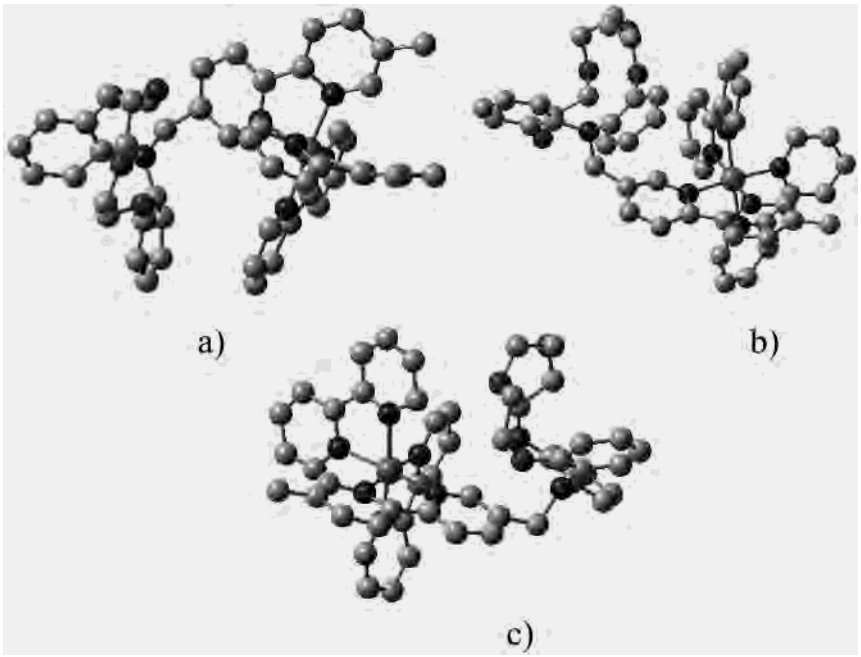

Figure 2. Three views taken from the molecular dynamics simulations run for the energy-minimized structure of the luminophore-appended crown ether. Hydrogen atoms have been omitted for clarity of presentation.

assignment of the chemical shift for the methylene groups of the crown ether. Likewise, correlation seen between H11 and H12 confirms the trans to cis isomerization of the bipyridyl arm accompanying coordination of the ruthenium center.

Molecular Dynamics Simulations. The molecular structure of $[Ru(bipy)_2(\mathbf{1})](PF_6)_2$ was computed and subjected to a molecular dynamics simulation (MDS) run in vacuo. Although a great number of conformations were sampled during the simulation, it was noticed that most structures could be assigned to one of three families. Thus, the most favorable structure (Figure 2a) has one of the amino phenylene rings held within 4 Å of an unsubstituted bipy moiety, with the two aromatic groups oscillating around a coplanar orientation. A second group of conformations (Figure 2b) involves the substituted bipy moiety remaining in fairly close proximity (i.e., 4−5 Å) of one of the amino phenylene rings. In this case, the two aromatic groups remain at a mutual angle of ca. 65° and do not adopt cofacial arrangements. The third family of conformations, which is the least favored, positions the two amino phenylene rings as far as possible from the metal complex (Figure 2c). This has the effect of pushing the crown ether closer to the metal complex while keeping the N lone pair away from the substituted bipy fragment. Throughout the entire simulation the distance between the amino N atom and the closest C atom of the metal complex lies within the range 2.25−3.00 Å. Overall, the molecular dynamics simulations appear to be consistent with the results of the NMR studies.

Photophysical and Electrochemical Properties. The absorption spectrum of the metal complex in dilute acetonitrile solution is presented in Figure 3. An intense absorption band centered at 288 nm ($\epsilon = 78400\ M^{-1}\ cm^{-1}$) can be attributed to $\pi \rightarrow \pi^*$ transitions localized on the bipy moieties. In the visible region, the well-documented[28] metal-to-ligand, charge-transfer (MLCT) transition associated with the metal complex is centered at 450 nm ($\epsilon = 11830\ M^{-1}\ cm^{-1}$). Emission, attributable to the lowest-energy, MLCT excited triplet state, is readily apparent in deoxygenated acetonitrile at ambient temperature. The emission maximum is located at 625 nm, and the absolute quantum yield, measured using $[Ru(bipy)_3](PF_6)_2$ as a reference, is 0.070 ± 0.010. The excited-state lifetime, also recorded in deoxygenated acetonitrile at room temperature, was found to be 365 ± 15 ns. These values are within the range found for many substituted ruthenium(II) poly(pyridine) complexes while it is noticeable that the decay kinetics remained strictly monoexponential at all monitoring wavelengths. The triplet−triplet differential absorption spectrum (Figure 4) shows strong bleaching of the MLCT absorption band around 460 nm, together with positive absorption at longer and shorter

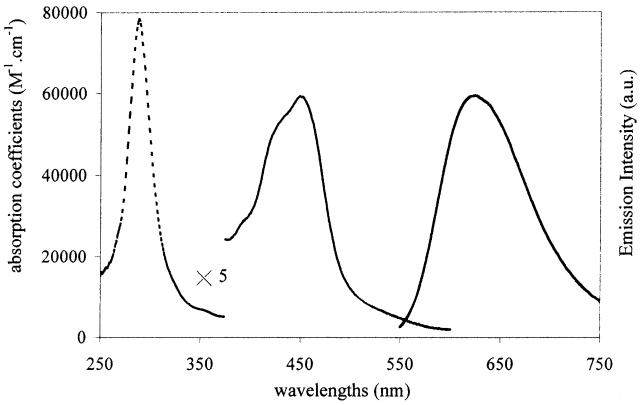

Figure 3. Absorption and emission spectra recorded for $[Ru(bipy)_2 \cdot \mathbf{1}](PF_6)_2$ in deoxygenated acetonitrile at ambient temperature.

(28) Juris, A.; Balzani, V.; Barigelletti, F.; Campagna, S.; Belser, P.; von Zelewsky, A. *Coord. Chem. Rev.* **1988**, *84*, 85.

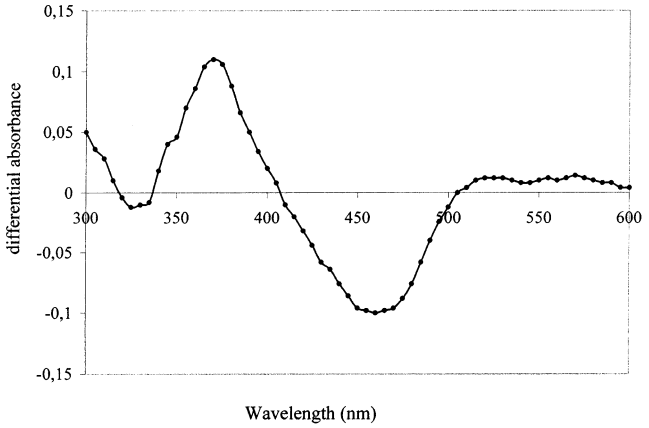

Figure 4. Differential transient absorption spectrum recorded for [Ru(bipy)$_2$·**1**](PF$_6$)$_2$ in deoxygenated acetonitrile at room temperature.

Table 2. Electrochemical Properties Recorded for the Various Systems[a]

complex	$E_{1/2}$ (ox, soln), V (ΔE_p, mV); E_{pa}, V[b]	$E_{1/2}$ (red, soln), V (ΔE_p, mV)[c]
Ru(**1**)	+1.28 (80); E_{pa} = +0.98	−1.38 (65), −1.58 (65), −1.89 (70)
Ru(**1**) + 100 equiv of Li$^+$ [c]	+1.25 (70); E_{pa} = +0.94	
Ru(**1**) + 100 equiv of Na$^+$ [d]	+1.27 (70); E_{pa} = +0.96	
Ru(**1**) + 100 equiv of CF$_3$COOH[e]	+1.25 (70)	
[Ru(bipy)$_3$]$^{2+}$	+1.27 (70)	−1.34 (70), −1.54 (70), −1.79 (75)
3	E_{pa} = +0.86	
3 + 100 equiv of CF$_3$COOH	E_{pa} = +0.84	
3 + 100 equiv of Li$^+$	E_{pa} = + 1.01	
2	E_{pa} = +0.89	

[a] Electrolyte used was 0.1 M TBAPF$_6$/anhydrous acetonitrile, concentration 0.15 mM, at room temperature for Ru(**1**) and 0.1 M TBAPF$_6$/anhydrous dichloromethane, concentration 0.2 mM, at room temperature for **2** and **3**. All potentials (±10 mV) are reported in V vs SSCE and using Fc$^+$/Fc (+0.38 V) as internal standard. Scan rate: 200 mV s^{-1}. $E_{1/2} = (E_{pa} + E_{pc})/2$; E_{pa} and E_{pc} are peak anodic and peak cathodic potentials, respectively. [b] E_{pa} refers to the anodic peak potential for the irreversible oxidation wave belonging to the appended diarylaza crown ether fragment. [c] Added as hydrated LiClO$_4$. The cathodic part of the voltammogram is masked by water reduction. [d] Added as hydrated NaClO$_4$. The cathodic part of the voltammogram is masked by water reduction. [e] Added as as pure acid. The cathodic part of the voltammogram is masked by proton reduction.

wavelengths that can be attributed to the bipy π-radical anion. The crown ether does not contribute toward absorption or emission processes at the wavelengths considered here.

Cyclic voltammograms recorded for the metal complex and the corresponding model compound **3** were recorded in acetonitrile and dichloromethane, respectively, with TBAP (0.2 M) as background electrolyte. Scan rates ranged from 50 to 1000 mV/s, and the difference in peak potentials between forward and reverse sweeps at zero scan rate (ΔE_p) was extrapolated from plots of ΔE_p versus the square root of the scan rate. The derived values are collected in Table 2 and referenced to the SSCE electrode, together with the ΔE_p values for all the redox processes. Crown ether **3** was found to exhibit an irreversible oxidation peak centered at +0.86 V. Interestingly, progressive addition of anhydrous CF$_3$-COOH (1−100 molar equiv) caused the peak to undergo a slight shift but also a significant decrease in peak current (Figure 5). In fact, the peak disappeared in the presence of a large excess of acid. Since it is expected that protonation of the secondary amine will inhibit its oxidation, we can infer that the oxidative process seen at +0.86 V refers to the amino N atom and not the aromatic groups of the crown ether.

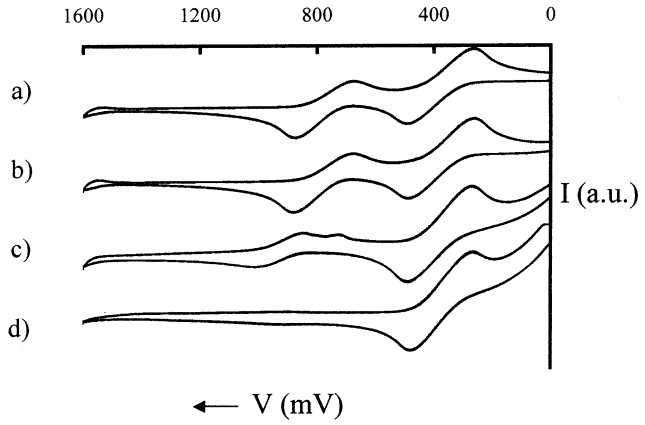

Figure 5. Cyclic voltammogramm recorded for derivative **3** in deoxygenated dichloromethane containing 0.01 M TABP as supporting electrolyte: (a) without CF$_3$COOH; (b) with 10 equiv of CF$_3$COOH; (c) with 100 equiv of CF$_3$COOH; (d) with 1000 equiv of CF$_3$COOH.

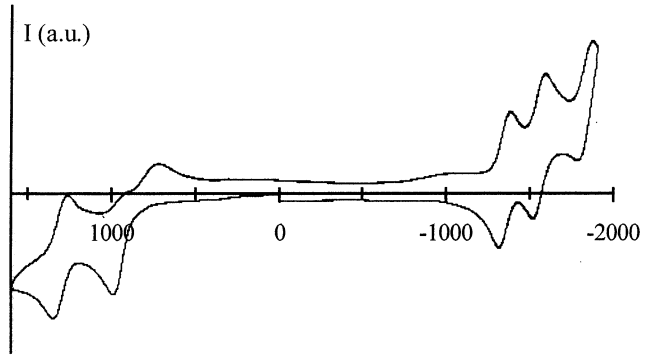

Figure 6. Cyclic voltammogram recorded for [Ru(bipy)$_2$·**1**](PF$_6$)$_2$ in deoxygenated acetonitrile containing 0.01 M (*n*-Bu)$_4$N·PF$_6$ as supporting electrolyte.

Since it is known that structural effects can exert a pronounced effect on the redox properties of crown ethers, we have also recorded the electrochemical properties of **2**. Similar oxidative behavior was observed, with an irreversible oxidation peak centered +0.89 V vs Fc/Fc$^+$. However, numerous small peaks were also apparent on the reverse sweep. These latter signals are tentatively assigned to decomposition products. Progressive addition of CF$_3$COOH caused the familiar shift of the anodic peak and its total extinction in strongly acidic media.

Cyclic voltammograms recorded for [Ru(bipy)$_2$(**1**)]$^{2+}$ display two peaks at positive potentials (Figure 6). Following from the electrochemical behavior of **3**, the first irreversible anodic peak can be assigned to oxidation of the tertiary amine. This process is anodically shifted by 120 mV in the complex due to electrostatic repulsion by the positively charged metal center. The second oxidative process is quasi-reversible and can be attributed to one-electron oxidation of the metal center. The derived reduction potential remains

Table 3. Triplet Lifetime Measured for the Ruthenium(II) Poly(pyridine) Chromophore in Deoxygenated Acetonitrile upon Addition of Various Cations (Added as Their Perchlorate Salt)

cation	τ (ns)	$[M^+]$ (mmol)
–	365	
H^+ [a]	690	59
Li^+	470	14
Na^+	535	21
K^+	425	13
Zn^{2+}	380	11

[a] Added as HCl at 36% in water.

comparable to that found for the parent complex, $[Ru(bipy)_3]^{2+}$, thereby indicating that the donating effect of the alkyl groups does not perturb the electronic properties of the metal center. The reversibility of this process is indicated by the fact that forward and reverse peak currents are essentially equal while ΔE_p is ca. 60 mV.[29] As expected on the basis of earlier work with the parent metal complex, three well-resolved, reversible, one-electron-reduction steps are apparent in the cyclic voltammograms. The derived reduction potentials remain similar to those recorded for $[Ru(bipy)_3]^{2+}$,[28,29] and as such they can be assigned to progressive reduction of the bipy ligands. Since the third reduction peak is shifted more cathodic by ca. 100 mV relative to the parent, we conclude that this step refers to one-electron reduction of the substituted bipy group.

As noted above, addition of excess CF_3COOH resulted in complete disappearance of the anodic peak assigned to one-electron oxidation of the tertiary amine. However, addition of $LiClO_4$ or $NaClO_4$ (5−100 molar equiv) to a solution of $[Ru(bipy)_2(\mathbf{1})]^{2+}$ in acetonitrile containing the background electrolyte had little, if any, effect on the electrochemistry. Identical electrochemical behavior was noted for **3**, and it is clear that excess cation does not seriously perturb the oxidative properties of the amino N atom.

Cation Binding. The $[Ru(bipy)_2(\mathbf{1})]^{2+}$ complex has been designed with a view to bind adventitious cations at the crown ether and in anticipation that the binding process could be registered by a change in the luminescence properties of the appended metal poly(pyridine) complex. However, it was found that addition of a large excess of Li^+, Na^+, or K^+ had no obvious effect on the absorption spectrum of $[Ru(bipy)_2(\mathbf{1})]^{2+}$ in dilute acetonitrile solution at room temperature. This situation could arise because the binding constant for cation coordination is weak or because binding does not perturb the electronic properties of the emissive metal complex. In contrast, it was noted that addition of alkali metal perchlorates caused a modest but definite increase in the triplet lifetime of $[Ru(bipy)_2(\mathbf{1})]^{2+}$ in deoxygenated acetonitrile solution (Table 3). Since cation binding does not affect the absorption spectrum in the region of the spin-forbidden transitions, it is concluded that coordination must decrease the rate of one or more nonradiative decay processes.

The ability of complexed cations to enhance the emission yield from the appended luminophore was confirmed by spectroluminescence titrations carried out in acetonitrile solution. These titrations required high concentrations of cation (H^+, K^+, Na^+, Li^+), delivered as the hydrated perchlorate salts, in order to effect changes in the luminescence intensity. Under these conditions, the addition of cation enhanced the luminescence quantum yield, without affecting the absorption spectrum. Addition of equivalent amounts of tetraethylammonium perchlorate or water had no effect on the emission yield of the ruthenium(II) complex. It was noted, however, that very high concentrations of cation were needed to effect complete binding. Thus, spectroluminescence titrations carried out with Li^+ as the added cation showed that the binding constant for formation of a 1:1 complex was only 23 ± 4. Addition of further quantities of $LiClO_4$ led to increased emission from the luminophore (Figure 7), but it was not possible to maintain a constant ionic strength under such conditions.

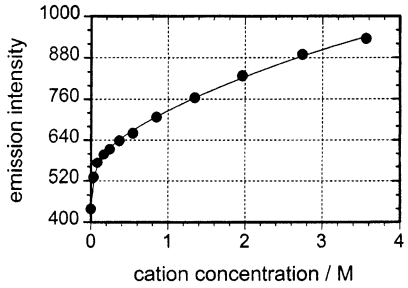

Figure 7. Typical spectroluminescence titration recorded for the successive addition of $LiCLO_4$ to a solution of $[Ru(bipy)_2\cdot\mathbf{1}](PF_6)_2$ in deoxygenated acetonitrile. The solid line drawn through the data points refers to a least-squares best fit to a binding constant of $K = 23$.

Additional evidence for complexation between the crown ether and alkali metal perchlorates was sought from ^1H NMR spectroscopy and cyclic voltammetry. In the NMR studies, the most significant changes were observed when small cations like Li^+ or H^+ were added to the $[Ru(bipy)_2(\mathbf{1})]^{2+}$ complex in CD_3CN. Thus, complexation of Li^+ was investigated using solutions with 0, 1, 10, and 40 molar equiv of $LiClO_4\cdot 3H_2O$ added to the solution. These spectra reveal gradual changes in certain chemical shifts, especially those due to the aromatic protons and to protons on the methylene bridge (Figure 8). With increasing Li^+ concentration, the methylene protons shift progressively toward high field and ultimately give rise to an AB spin system centered at 4.53 ppm. This finding is consistent with cation attachment rigidifying the crown ether, thereby allowing a distinction between the diastereotopic methylene protons. The most relevant changes in the aromatic region are due to protons associated with the phenylene rings ($6.6 < \delta < 7.0$ ppm for the free chromophore). In the absence of Li^+, this latter region of the spectrum comprises two sets of peaks, each of which corresponds to two protons. Upon addition of excess Li^+, this pattern undergoes an upfield shift of 0.09 ppm for H4 and downfield shifts of 0.11, 0.13, and 0.28 ppm, respectively, for H5, H6, and H7. These shifts are considered to be characteristic of cation binding. Complexation also causes the appearance of a broad singlet centered at 7.19 ppm.

Again, 2-D COSY and NOESY studies facilitated assignment of all the protons associated with the complexed crown

(29) Bard, A.; Faulkner, L. R. In *Electrochemical Methods, Fundamentals and applications*; John Wiley and Sons: New York, 1980.

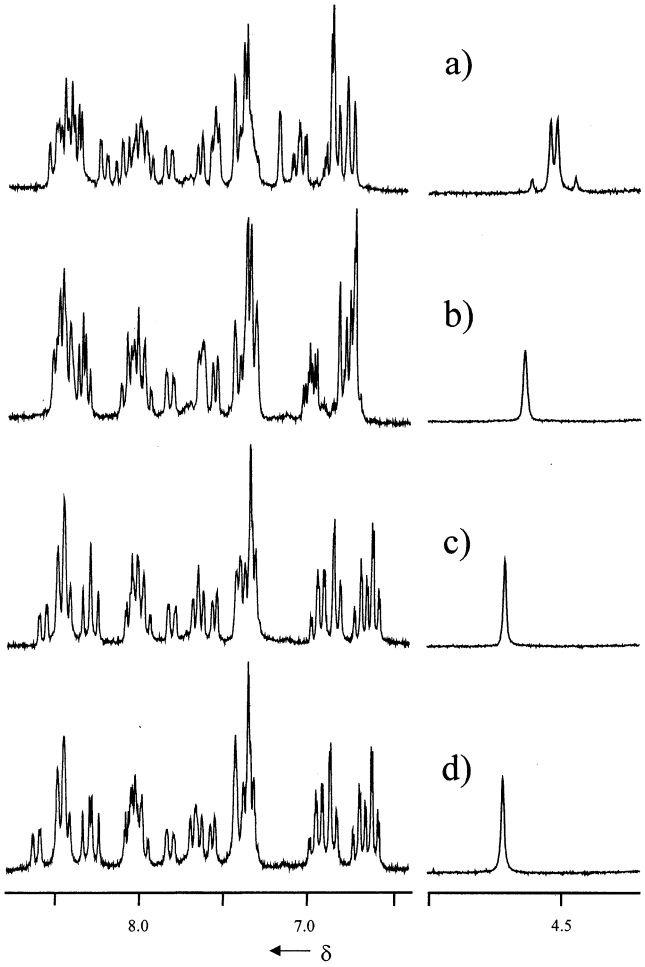

Figure 8. Evolution of the ^{1}H NMR spectrum recorded for $[Ru(bipy)_2(\mathbf{1})](PF_6)_2$ upon addition of 40, 10, 1, and 0 equiv (respectively a, b, c, and d) of $LiClO_4 \cdot 3H_2O$.

ether. The results collected in the presence of excess Li^+ are given in Table 1. While H9 and H15 are isochronous in the free crown ether complex, complexation of Li^+ to the crown ether causes their degeneracy to be lost. A COSY correlation between H14 and H15 shows that H15 remains unperturbed while H9 is shifted upfield by 0.24 ppm and appears as the new singlet at 7.19 ppm. Furthermore, the NOESY spectra clearly indicate a correlation between H9 and H7, which in turn shows that the ruthenium core lies beside the phenyl rings.

Molecular dynamics simulations run in a bath of acetonitrile molecules indicate that encapsulation of a Li^+ cation within the crown ether leads to a distinct rigidification of the molecular conformation, as shown by NMR. The average conformation for the cation complex (Figure 9) has the Ru(II) and Li^+ cations situated as far apart as possible (i.e., 9.8 Å), presumably to minimize electrostatic repulsion. This structure directs the crown ether away from the luminophore. The two amino phenylene rings point away from the substituted bipy moiety while the amino N lone pair remains ca. 2.5 Å from a C atom on the substituted bipy ligand. The molecule does not adopt cofacial arrangements. Interestingly, the energy-minimized structure reveals that the bound Li^+ is positioned ca. 3.4 Å from the amino N atom. This seems

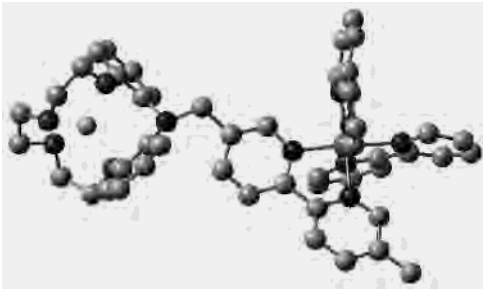

Figure 9. Energy-minimized structure for the Li^+ cation complex. Hydrogen atoms and solvent molecules have been omitted for clarity of presentation.

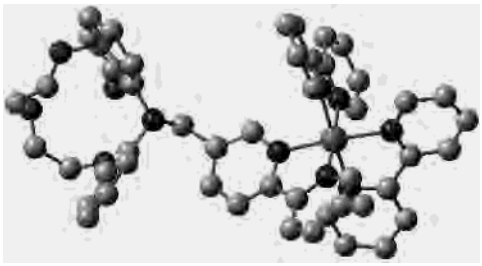

Figure 10. Energy-minimized structure for the protonated species. The hydrogen atoms have been omitted for clarity of presentation. Note: The added proton is attached to the amino N atom and points toward the viewer.

rather long for a Li^+-N bond. However, the MDS's indicate that the Li^+-N distance varies from 2.0 to 4.0 Å while the Li^+-O distance covers the range 1.75−3.75 Å. At any given time, three O atoms are close (i.e., <2.5 Å) to the cation. This picture is consistent with the bound Li^+ cation sampling a variety of coordination geometries but with the amino N atom playing an insubstantial role.

Addition of protons to a solution of $[Ru(bipy)_2(\mathbf{1})]^{2+}$ in CD_3CN results in a very complicated ^{1}H NMR spectrum. The only indentifiable spectral change concerns the methyl group of the appended bipyridyl unit which splits into two singlets at 2.16 and 2.20 ppm. This fact is in agreement with our expectation of two isomeric forms of the ammonium salt, with the $[Ru(bipy)_3]^{2+}$ core being directed toward or away from the crown ether. Molecular dynamics simulations made for the protonated species indicate that the proton resides outside the cavity defined by the crown ether (Figure 10). The structure seems to be set by the need to minimize electrostatic repulsion.

Discussion

It should be recognized that the triplet lifetime recorded for $[Ru(bipy)_2(\mathbf{1})]^{2+}$ (τ_T = 365 ns) in deoxygenated acetonitrile is shorter than that recorded for the parent complex (τ_T = 950 ns) under identical conditions. This quenching effect is most likely due to intramolecular electron transfer from the nearby N atom to the triplet state of the metal complex. The rate constant for this process can be estimated at ca. 1.7×10^6 s^{-1} while the free energy difference of the process is very crudely estimated to be ca. +0.26 eV. This latter value is simply taken as the difference between the relevant peaks in the cyclic voltammograms (ΔE_p = 2.36 eV), ignoring the irreversibility of the amine oxidation step, and the triplet energy (E_T = 2.1 eV) measured from the

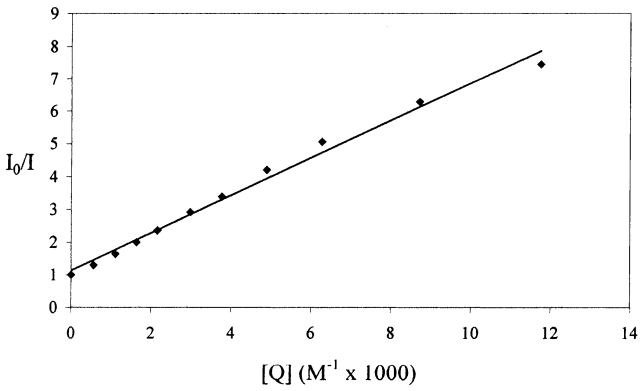

Figure 11. Stern−Volmer plot for quenching of $[Ru(bipy)_3]^{2+}$ by compound **3** in air-equilibrated dichloromethane.

emission spectrum. It was not possible to detect the anticipated redox products as transient species in the laser flash photolysis records, but it is reasonable to suppose that charge recombination ($\Delta G° = -2.4$ eV) is much faster than charge separation. The relatively slow triplet quenching reaction seems consistent with the restricted driving force.

The viability of photoinduced electron transfer from the amino donor to the triplet excited state of the metal complex was confirmed by a separate experiment in which the diarylaza crown ether **3** was found to be a quencher for emission from the parent complex, $[Ru(bipy)_3](PF_6)_2$, in dichloromethane solution. Bimolecular quenching followed Stern−Volmer behavior[30] (Figure 11) and gave a quenching rate constant of 1.4×10^9 M^{-1} s^{-1}. This latter value is reminiscent of bimolecular quenching rate constants observed with other arylamines[31,32] and is reduced from the diffusion-controlled rate limit by a factor of ca. 10-fold. The corresponding intramolecular process seems to be much less efficient, but this is easily rationalized in terms of thermodynamic and stereochemical aspects. Thus, the amino group in **3** is easier to oxidize than that in $[Ru(bipy)_2{\cdot}\mathbf{1}]^{2+}$, due to electrostatic effects, while the intervening organic framework does not permit close approach between the Ru(II) center and the amino N atom in $[Ru(bipy)_2{\cdot}\mathbf{1}]^{2+}$. The latter realization implies that electron transfer must involve either tunneling through the connecting methylene group or long-range, through-space interactions. In fact, the MDS work indicates that the closest approach between the amino N atom and the Ru(II)/(III) cation is ca. 5.25 Å. The availability of conformations such as that shown in Figure 2a, where there is cofacial alignment of the aromatic groups, provides an alternative pathway for electron tunneling between the redox-active subunits.

(30) A τ_0 value of 413 ns has been measured in non-degasssed dichloromethane.
(31) Encinas, S.; Bushell, K. L.; Couchman, S. M.; Jeffery, J. C.; Ward, M. D.; Flamigni, L.; Barigelletti, F. *J. Chem. Soc., Dalton Trans.* **2000**, 1783.
(32) Ballardini, R.; Varani, G.; Indelli, M. T.; Scandola, F.; Balzani, V. *J. Am. Chem. Soc.* **1978**, *100*, 7219.

Complexation of an added cation at the crown ether site causes enhancement of emission from the luminophore without affecting the absorption spectrum. This finding suggests that the binding event decreases the rate of intramolecular electron transfer. It is clear, however, from both NMR spectroscopy and the MDS work that cation binding rigidifies the molecular structure such that the two cationic centers remain as far apart as possible. This effect curtails alignment of the aromatic units into cofacial orientations and decreases orbital contact between the Ru(III) center and the N lone pair at the triplet level. The overall consequence of this conformational change will be to minimize the rate of through-bond and/or through-space electron transfer.

The situation concerning proton binding might be somewhat different in that the amino N atom is likely to be involved directly in the coordination step. This behavior is clear from the cyclic voltammetry results where protonation inhibits oxidation of the amino group. There are also indications in the NMR spectra that proton binding differs from cation binding. In this case, the enhanced luminescence that accompanies protonation is likely caused by an electronic effect.

Conclusion

We have synthesized a new member of the crown ether family that is easily derivatized with a luminescent reporter, such as in $[Ru(bipy)_2{\cdot}\mathbf{1}]^{2+}$. Weak electronic coupling, probably occurring via through-space interactions, between the luminophore and the connecting amino group decreases the extent of emission from the metal complex. The addition of alkali metal cations, notably Li^+, restores emission by way of curtailing intramolecular electron transfer. This latter effect most likely arises because cation binding favors rigid conformations that minimize electronic coupling between the redox-active partners. Structural information gleaned from NMR spectroscopy in the absence and presence of cations is well supported by molecular dynamics simulations. It is further shown that the bridging amino group can be protonated such as to render the N atom incapable of functioning as an electron donor. Further effort in this field will be directed toward the development of luminescence and electrochemical sensors capable of the selective recognition of neutral substrates.

Acknowledgment. This work was partially supported by the CNRS, the EPSRC, and the ECPM. The authors gratefully acknowledge the expertise of Mr Michel Schmitt in measuring the 2-D NMR spectra. R.F.Z. is very grateful to Johnson Matthey Chemicals for providing us some precious metals.

IC020671T